

# Inferring Domain of Interactions among Elements from Ensemble of Trajectories II. -Effects of finite length trajectories and external noise

Udoy S. Basak

*Graduate School of Life Science, Transdisciplinary Life Science Course,  
Hokkaido University, Kita 12, Nishi 6, Kita-ku, Sapporo 060-0812, Japan and  
Pabna University of Science and Technology, Pabna 6600, Bangladesh*

Sulimon Sattari

*Research Center of Mathematics for Social Creativity,  
Research Institute for Electronic Science, Hokkaido University,  
Kita 20, Nishi 10, Kita-ku, Sapporo 001-0020, Japan*

Hossain M. Motaleb

*Research Center of Mathematics for Social Creativity,  
Research Institute for Electronic Science, Hokkaido University,  
Kita 20, Nishi 10, Kita-ku, Sapporo 001-0020, Japan and  
University of Dhaka, Dhaka 1000, Bangladesh*

Kazuki Horikawa

*Department of Optical Imaging, The Institute of Biomedical Sciences, Tokushima University Graduate School,  
3-18-15 Kuramoto-cho, Tokushima City, Tokushima, 770-8503, Japan*

Tamiki Komatsuzaki

*Research Center of Mathematics for Social Creativity,  
Research Institute for Electronic Science, Hokkaido University,  
Kita 20, Nishi 10, Kita-ku, Sapporo 001-0020, Japan  
Institute for Chemical Reaction Design and Discovery (WPI-ICReDD),  
Hokkaido University Kita 21 Nishi 10, Kita-ku, Sapporo, Hokkaido 001-0021, Japan  
Graduate School of Life Science, Transdisciplinary Life Science Course,  
Hokkaido University, Kita 12, Nishi 6, Kita-ku, Sapporo 060-0812, Japan and  
Graduate School of Chemical Sciences and Engineering Materials Chemistry and Engineering Course,  
Hokkaido University, Kita 13, Nishi 8, Kita-ku, Sapporo 060-0812, Japan*

Transfer entropy in information theory was recently shown [Phys. Rev. E 102, 012404 (2020)] to enable us to elucidate the interaction domain among interacting particles solely from an ensemble of trajectories. There, only pairs of particles whose distances are shorter than some distance variable, termed cutoff distance, are taken into account in the computation of transfer entropies. The prediction performance in capturing the underlying interaction domain is subject to noise level exerted on the particles and the sufficiency of statistics of the interaction events. In this paper, the dependence of the prediction performance is scrutinized systematically on noise level and the length of trajectories by using a modified Vicsek model. The larger the noise level and the shorter the time length of trajectories, the more the derivative of average transfer entropy fluctuates, which makes it difficult to identify the interaction domain in terms of the position of global minimum of the derivative of average transfer entropy. A measure to quantify the degree of strong convexity at coarse-grained level is proposed. It is shown that the convexity score scheme can identify the interaction distance fairly well even while the position of global minimum of the derivative of average transfer entropy does not.

## I. INTRODUCTION

Collective migration is the synchronized movement of agents emerging from the mutual interactions between them [1, 2]. One of the basic properties of collective motion is that the movement of an individual is influenced by the movement of other individuals in its local vicinity and/or through long range interactions, e.g., via some signals such as chemicals emitted by cells. At the cellular level, collective motion can be observed in wound healing, cancer development, and organogenesis [3–5]. The

question of how microscopic interactions between agents regulate the macroscopic group behavior is one of the most intriguing subjects [6]. This is closely related to the problem of causal inference within systems composed of many agents.

For the qualitative understanding of collective motion, a variety of simulation models have been proposed such as the Reynolds' flocking model [7], the Vicsek model (VM) [8], and the Couzin model [9]. Among these, the VM has been widely used to study various dynamics of collectively moving self-propelled particles, such as sym-

metry breaking [10, 11], phase transition [8, 12], and classification of leaders and followers [13, 14]. In the VM, each particle moves with a constant speed and its direction is determined by the average direction of motion of its neighboring particles in the presence of noise [15–17]. In other words, a moving particle interacts only with the particles within a distance of  $R$  as it would via direct interactions but also via signal transduction such as chemicals.

One of the possible drivers of collectively moving agents is the presence of influential individuals, sometimes referred to as ‘leaders’, who control the movement of the other individuals, referred to as the ‘followers’. Leader-follower relationships have been studied in a fish shoal [18], troops of baboons [19], in a colony of honey bee [20] and so forth. At the cellular level, it has been studied that collective migration of MDCK epithelial cells [21, 22], wound healing [23], cancer growth in breast [24], etc., are regulated by the leader cells.

Identifying leader and follower agents is a challenging endeavor. First and foremost, one must identify what it means to be a leader. Based on asymmetric nature of influence on activities among entities, in this article, we define a ‘leader’ as an entity which more influences (on average) on the activity of the other entities (termed ‘followers’). Once leadership has been defined, various types of empirical data, e.g., ensembles of trajectories of agents, can be used to infer the differential influence in interaction and identify leader-follower relationships. By definition, leaders are expected to be more persuasive compared to the followers. Since followers follow the movement of leaders, some correlation should exist between some physical quantity related to a leader and that related to a follower with a certain time delay, as information cannot travel from a leader to a follower at infinite speed.

To measure causal influence among multivariate time series, information theory provides a variety of approaches [25]. Some of the typical quantities used are mutual information [26], time-delayed mutual information [27], transfer entropy [27], and causation entropy [28]. These quantities have been computed using time lapse motion data of moving individuals to determine the directions of influence. For example, it was found by using a zebrafish interaction model that net transfer entropy is a more accurate classifier than extreme-event synchronization and cross-correlation for classifying leaders and followers [13]. In swarms of bats, transfer entropy was used to demonstrate that there exists a leader-follower relationship between the front bat and the rear bat [29]. Using the trajectories of handball players, it was showed that transfer entropy is capable of capturing the causal relationships between players [30].

In the above-mentioned studies, all pairs of agents are taken into account at every time instance to evaluate transfer entropy irrespective of the distance between the agents. This is not necessarily an optimal use of the data available for capturing the underlying leader-follower re-

lationship, given that the interaction domain is known. It was shown, using a modified VM, that the classification scores of leaders and followers significantly increase upon incorporating the identified interaction domain information compared to the conventional way of transfer entropy estimation where the distance between the agents is not taken into account [31]. When two particles come into their interaction domain, they may share or transfer information which results in some change in their motion such as the direction of motion. As the distance between them exceeds the interaction radius, the amount of information flow decreases and goes to zero at the limit of the distance being infinity in a fluctuating environment. This methodology requires that the interaction domain is known, which may not be the case. A new scheme has been proposed to estimate the underlying interaction domain from the trajectories of particles to monitor the change in transfer entropy as a function of the distance between them, called cutoff distance  $\lambda$ . It was demonstrated that the derivative of average transfer entropy (and also cross correlation) with respect to  $\lambda$  has a minimum near the interaction domain, by which one can identify the underlying interaction domain from a set of trajectories [31].

The scheme is dependent on how transfer entropy can be estimated so that it takes into account enough statistics of interacting particles, and positions and numbers of the minimum of the derivative of average transfer entropy along the cutoff distance  $\lambda$  may also be subject to the extent of external noise and time length of trajectories. In this paper, we scrutinize how the prediction performance in capturing the underlying interaction domain depends on the size of noise and time length of the trajectory data. We also examine an alternative scheme expected to be stable against noises and time length, that relies on the degree of convexity at coarse-grained scale in the derivative of average transfer entropy along the cutoff distance, and time variance of underlying interaction radius of particles.

## II. IDENTIFICATION OF LEADERS AND FOLLOWERS

Transfer Entropy (TE) from time series of a stochastic variable  $X = \{\dots, x_{t-1}, x_t, x_{t+1}, \dots\}$  to time series of another stochastic variable  $Y = \{\dots, y_{t-1}, y_t, y_{t+1}, \dots\}$  is defined as [27]:

$$\begin{aligned} TE_{X \rightarrow Y} &= I(y_{t+\tau}; x_t | y_t), \\ &= \sum_{y_{t+\tau}, y_t, x_t} p(y_{t+\tau}, y_t, x_t) \log_2 \left( \frac{p(y_{t+\tau} | y_t, x_t)}{p(y_{t+\tau} | y_t)} \right), \\ &= H(y_{t+\tau} | y_t) - H(y_{t+\tau} | y_t, x_t), \end{aligned} \quad (1)$$

where  $\tau$  is the time lag between the two time instants and  $H(\cdot)$  represents the conditional Shannon entropy [26]. TE is proven to be non-negative. A positive value of  $TE_{X \rightarrow Y}$  is considered to indicate the causal influence

of  $X$  on  $Y$  [32]. For a pair of agents  $X$  and  $Y$ , the net transfer entropy from  $X$  to  $Y$ , defined as  $NTE_{X \rightarrow Y} = TE_{X \rightarrow Y} - TE_{Y \rightarrow X}$  can be used to infer the direction of causal influence. A positive  $NTE_{X \rightarrow Y}$  may indicate that  $Y$  follows  $X$ , which quantifies the causal direction from  $X$  to  $Y$ .

As a classifier to differentiate leaders and followers, the average net transfer entropy is used, which is denoted as  $\chi$  and defined for a given particle  $i$  as follows:

$$\chi^{(i)} = \frac{1}{N-1} \sum_{j(\neq i)} (TE_{i \rightarrow j} - TE_{j \rightarrow i}),$$

where  $TE_{i \rightarrow j}$  represents TE from the particle  $i$  to  $j$  and  $N$  is the total number of particles in the system. The value of  $\chi^{(i)}$  for each particle  $i$  is compared to a selected threshold value  $\epsilon$ . A particle for which  $\chi^{(i)}$  is higher than the threshold  $\epsilon$  is identified as a leader, otherwise it is identified as a follower. The resulting classification is compared to the ground truth to obtain the true-positive rate and the false-positive rate for the chosen  $\epsilon$ . To show the classification performance of a classifier receiver-operating characteristic curve is used. It is obtained by plotting the true positive rate versus false positive rate at different values of  $\epsilon$  [13]. In order to quantify the accuracy of the classifier's performance and to compare the performance of different classifiers, area under receiver-operating characteristic curve (AUC) has been used [33]. An AUC score of 1.0 means that that classifier accurately predicts the identities of the particles whereas a value of 0.5 means that the classifier has no class separation capacity whatsoever.

### III. MODIFIED VICSEK MODEL

Similar to the standard VM [8], we consider that  $N$  self-propelled particles are moving with the same constant speed  $v_0$  in a two-dimensional square box of length  $L$  with periodic boundary conditions, and at time  $t = 0$  the particles are positioned and oriented randomly. At time  $t + 1$ , the position of  $i$ th particle is denoted by  $\vec{r}_i^{t+1}$  is updated at each time step  $\Delta t$  as:

$$\vec{r}_i^{t+1} = \vec{r}_i^t + \vec{v}_i^t \Delta t, \quad (2)$$

where  $\vec{r}_i^t$  denotes the position of  $i$ th particle at time  $t$ , and  $\vec{v}_i^t$  represents the corresponding velocity of the particle with an absolute speed  $v_0$  and a direction given by the angle  $\theta_i(t)$ . This angle is obtained from the following equation:

$$\theta_i(t+1) = \langle \theta(t) \rangle_{R, w, \vec{r}_i^t} + \Delta \theta_i. \quad (3)$$

Here  $\langle \theta(t) \rangle_{R, w, \vec{r}_i^t}$  is the weighted orientation averaged over particles (including the particle  $i$  itself), which are within a circle of radius  $R$  centered on the position  $\vec{r}_i^t$  of the particle  $i$  at time  $t$ , computed

by  $\arctan \left[ \frac{\sum_j' w_{ji} \sin \theta_j(t)}{\sum_j' w_{ji} \cos \theta_j(t)} \right]$  where  $\sum_j'$  takes over all  $j$  satisfying  $|\vec{r}_i^t - \vec{r}_j^t| \leq R$  [31].  $w$  is a matrix whose element  $w_{ij}$  corresponds to the interaction strength that the particle  $i$  exhibits on its neighboring particle  $j$ . If the particle  $i$  is a leader and  $j$  is a follower, then  $w_{ij} > w_{ji}$ . Also the interaction strength of a particle  $i$  on itself is 1.0 i.e.,  $w_{ii} = 1.0$ . We set the values of leaders' and followers' interaction strengths to 1.05 and 1.00, respectively.  $\Delta \theta_i$  represents random number at time  $t$  which can be chosen with a uniform probability distribution from the interval  $[-\eta_0/2, \eta_0/2]$ , where  $\eta_0$  may be considered as a temperature-like parameter. The total time length is designated by  $T$  during which transfer entropies are estimated between leader and follower particles.

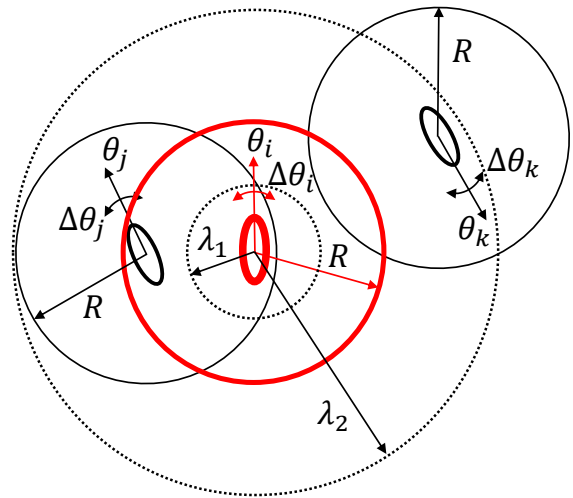


Figure 1. Schematic diagram of cutoff distance. Ovals represent moving particles.  $\theta_i$ ,  $\theta_j$ , and  $\theta_k$  represent the direction of motion of receptive particles at time  $t$  and  $R$  is the interaction radius.  $\lambda_1$  and  $\lambda_2$  exemplify two different cutoff distances. For example, for the cutoff distance  $\lambda = \lambda_1$ , the actual distance between the particles  $i$  and  $j$  at this time instance is larger than  $\lambda_1$ , and hence, their orientation information is not considered for TE calculation between them even though the particles are located within each other's interaction domain (likewise the orientational information between the particle  $i$  and  $k$  is not taken into account in the computation of TE at  $\lambda = \lambda_1$ ). But for  $\lambda = \lambda_2$ , particles  $j$  and  $k$  are both located within the distance of  $\lambda_2$  from particle  $i$ . Hence the orientation information of  $\theta_k$  and  $\theta_i$  and that of  $\theta_j$  and  $\theta_i$  are considered to compute TE irrespective of the underlying interaction radius  $R$ .

In the VM each particle moves with a constant speed  $v_0$ . In this paper the value of  $v_0$  is set to be 0.3 arb. units. It was found that in the range of  $0.05 \leq v_0 \leq 0.9$  the classification scores of leader and follower were almost the same. Though the speed is the same for all particles, particles change their direction of motion over time. In case of a leader-follower pair of particles, because of the domination of the leader, the follower particle changes its direction towards the leader's headings. Hence orienta-

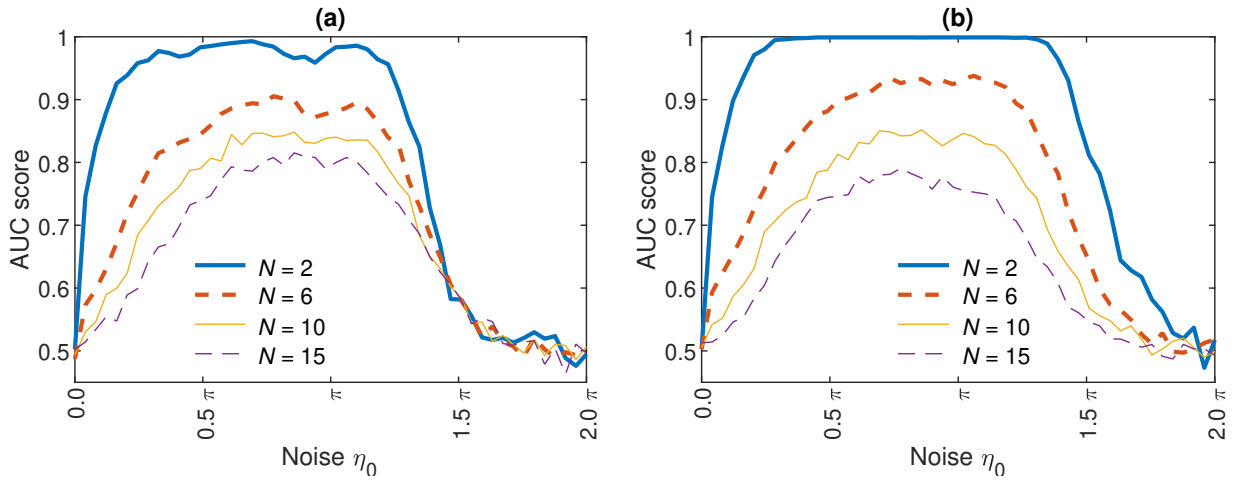


Figure 2. Classification scores of different numbers of particles at different noise levels. (a) Fixed box size. Density changes with different number of particles:  $\rho = 0.02$  arb. units ( $N = 2$ ),  $0.06$  ( $N = 6$ ),  $0.10$  ( $N = 10$ ), and  $0.15$  ( $N = 15$ ). (b) Fixed density as  $0.1$  arb. units. Box size changes with different number of particles:  $L = 4.47$  arb. units ( $N = 2$ ),  $7.75$  ( $N = 6$ ),  $10$  ( $N = 10$ ), and  $12.25$  ( $N = 15$ ).

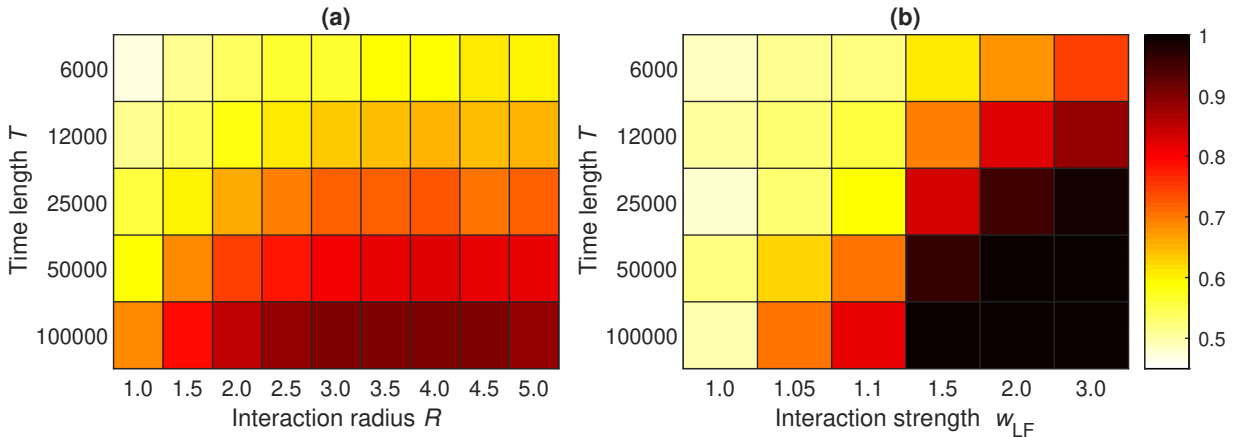


Figure 3. AUC landscape at different time length for different interaction radius and interaction strength. (a) AUC landscape corresponds to  $\eta_0 = 1.2\pi$  arb. units and  $w_{LF} = 1.05$  arb. units. AUC value increases as the time length and interaction radius  $R$  increase. (b) AUC landscape correspond to  $\eta_0 = 1.2\pi$  and  $R = 1$ . For this analysis  $w_{FL} = 1$  is fixed and  $w_{LF}$  were varied. Similar behaviors were observed at other noise levels (not shown).

tion of particles is used to compute transferred information between them. In this paper, the orientation space  $[0 : 2\pi]$  is discretized into six bins of equal size which are represented by unique symbols [31].

In Eq. (3) the orientation of the particle  $i$  at time  $(t + 1)$  depends largely on the orientation of itself and nearby particles at time  $t$ . The delay time  $\tau$  is set to be 1 for the estimation of TE throughout this paper. All analyses were performed with 1000 realizations and for each realization the values of  $\vec{r}_i^t$  and  $\vec{r}_i^{t+1}$  at time  $t = 0$  are chosen randomly in Eq. (2). In this paper box size  $L$ , number of particles  $N$ , time length  $T$ , interaction radius  $R$ , are varied to check their effect on classification score.

#### IV. CUTOFF DISTANCE

Knowledge of the interaction domain greatly improves the classification of leaders and followers. In practice, however, one does not know the interaction domain for a group of animals, cells, or birds a priori. To deduce it from an ensemble of trajectories, the ‘cutoff distance variable’  $\lambda$  was introduced [31]. In this problem setting, the interaction domain is considered as a circle of radius  $R$ , which is unknown, however, in general the same technique can be applied to infer an interaction domain of any shape. Then for the estimation of TE, the cutoff distance  $\lambda$  is defined as a distance up to which the interactions between particles are taken into consideration [Figure 1]. In other words, for the estimation of TE from the ‘symbolic time series’ of a particle to another, the

probability distributions are estimated only at the time instance  $t$  when the distance between those two particles is less than the cutoff distance  $\lambda$ . Finally the value of  $\lambda$  is varied and TE between particles is computed as a function of  $\lambda$ . Whenever there is no mention of a cutoff distance  $\lambda$ , e.g. in Section V, it means that the distance information between particles is not considered which is the conventional way of TE computation [13, 29].

## V. RESULTS AND DISCUSSIONS

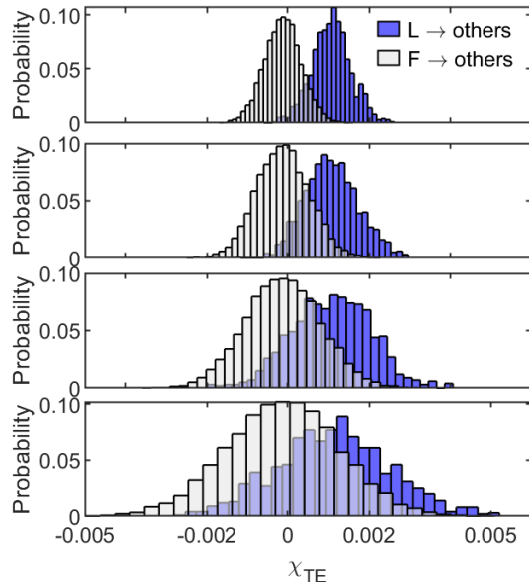


Figure 4. Distributions of the classifiers  $\chi_{TE}$  (/bits) from the leader to the others, and those from a follower to the others for  $R = 3$ ,  $\eta_0 = 1.2\pi$ , and (a)  $T = 100,000$  arb. units, (b)  $T = 50,000$ , (c)  $T = 25,000$ , and (d)  $T = 12,000$ .

Figure 2 shows the AUC classification score (=the extent of how leader and followers are correctly classified from their orientation dynamics) with different numbers of particles  $N$  and noise levels  $\eta_0$ . Here, only one particle serves as a leader and the other  $(N - 1)$  particles serve as followers, under the constraint of box size  $L$  [Fig. 2(a)] or density  $\rho$  [Fig. 2(b)]. At low noise level  $\eta_0 \sim 0$  and very high level  $\eta_0 > 1.5\pi$ , the distributions of transfer entropies  $\chi_{TE}$  from leader to follower and vice versa over 1000 realizations were found to significantly overlap with each other, which makes differentiation between leader and follower difficult. The low AUC at very low noise level arises from the fact that particles fall into some concerted motion very quickly dependent solely on initial configurations, resulting in insufficient sampling of orientational dynamics, and in turn the low AUC at very high noise arises from overshadowing of the interactions by random noises [31]. As the number of particles increases, the AUC score decreases in both fixed box size and fixed density cases. This is because, in any pair of

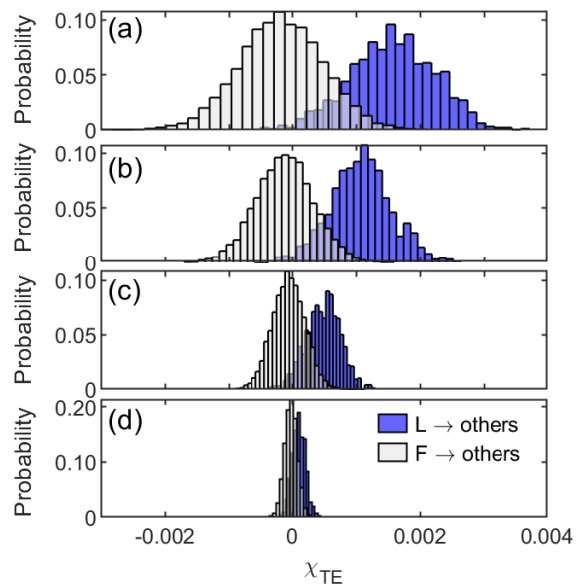


Figure 5. Distributions of the classifiers  $\chi_{TE}$  (/bits) from the leader to the others, and those from a follower to the others for  $T = 100,000$ ,  $\eta_0 = 1.2\pi$ , and (a)  $R = 4.0$ , (b)  $R = 3.0$ , (c)  $R = 2.0$ , and (d)  $R = 1.0$ .

particles for which TE is evaluated, their motions are also influenced by the other particles, and the more the number of particles increases, the more the motions of the particles in question are influenced by the third (or higher) particle. Compared the fixed box size case to the fixed density case, the AUC score for the fixed box size quickly drops to 0.5 (corresponding to a coin toss) around  $\eta_0 \sim 1.5\pi$  than those for the fixed density condition. It suggests that, as the density gets higher, the motion of particles in any pair are more influenced by additional particles.

The effects of time length  $T$ , interaction radius  $R$ , and leaders' interaction strength  $w_{LF}$  on classification score are shown in Fig. 3. In this analysis 10 particles were used, with one serving as a leader and the other 9 particles as followers. In Fig. 3(a) we varied time length  $T$  and interaction radius  $R$ . It is shown that the AUC score increases with  $T$  and  $R$ . For shorter  $T$ , due to insufficient sampling in characterizing leader-follower interaction relationship, the distributions of  $\chi_{TE}$  from leader to the others and from follower to the others have higher variance as shown in Fig. 4. As a result, it is difficult to distinguish leader and followers for short  $T$ . As  $T$  increases, due to more exploration of interaction events between leader and followers, the variance of leaders' and followers' distributions gets smaller, making the classification easier. Figure 5 shows, in turn, the interaction radius  $R$  dependency on distributions of the classifiers  $\chi_{TE}$ . Larger  $R$  allows particles to be taken into account in elucidating the leader-follower interaction relationship, which produces easily distinguishable distributions of leader and followers as shown in Fig. 5(a). In

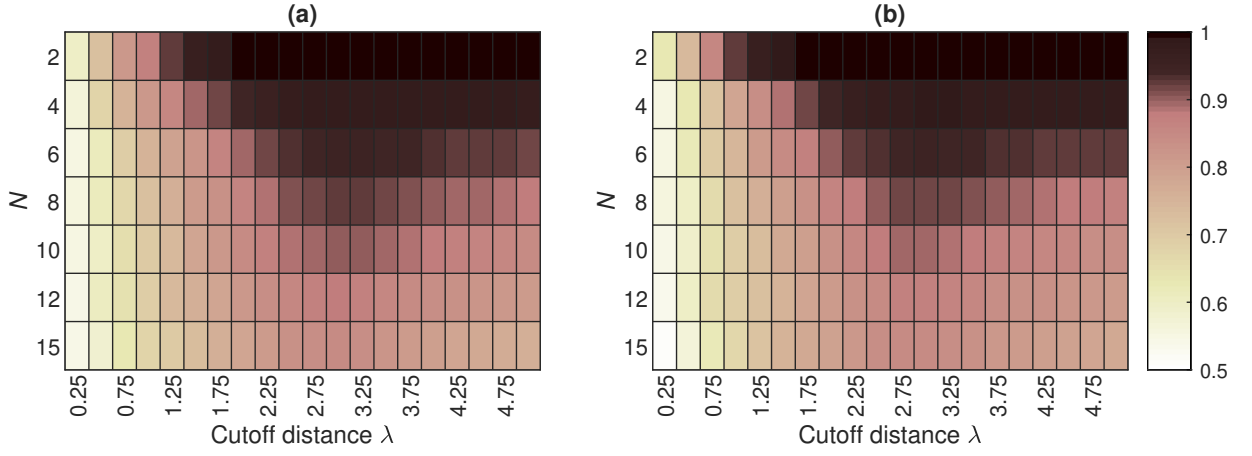


Figure 6. AUC landscape for different numbers of particles at different cutoffs. Actual interaction radius  $R$  used for the trajectory calculation is 3.0 and the noise is  $\eta_0 = \frac{\pi}{2}$ . (a) Fixed box size. The highest AUC scores and their locations are: 0.999 at  $\lambda = 3.25$  arb. units ( $N = 2$ ), 0.984 at  $\lambda = 3.25$  ( $N = 4$ ), 0.946 at  $\lambda = 3.0$  ( $N = 6$ ), 0.926 at  $\lambda = 3.25$  ( $N = 8$ ), 0.903 at  $\lambda = 3.0$  ( $N = 10$ ), 0.878 at  $\lambda = 3.0$  ( $N = 12$ ), and 0.846 at  $\lambda = 3.0$  ( $N = 15$ ). (b) Fixed density. The highest AUC scores and their locations are: 0.999 at  $\lambda = 3.0$  ( $N = 2$ ), 0.986 at  $\lambda = 3.25$  ( $N = 4$ ), 0.947 at  $\lambda = 3.0$  ( $N = 6$ ), 0.921 at  $\lambda = 3.0$  ( $N = 8$ ), 0.897 at  $\lambda = 3.0$  ( $N = 10$ ), 0.870 at  $\lambda = 3.0$  ( $N = 12$ ), and 0.851 at  $\lambda = 3.0$  ( $N = 15$ ).

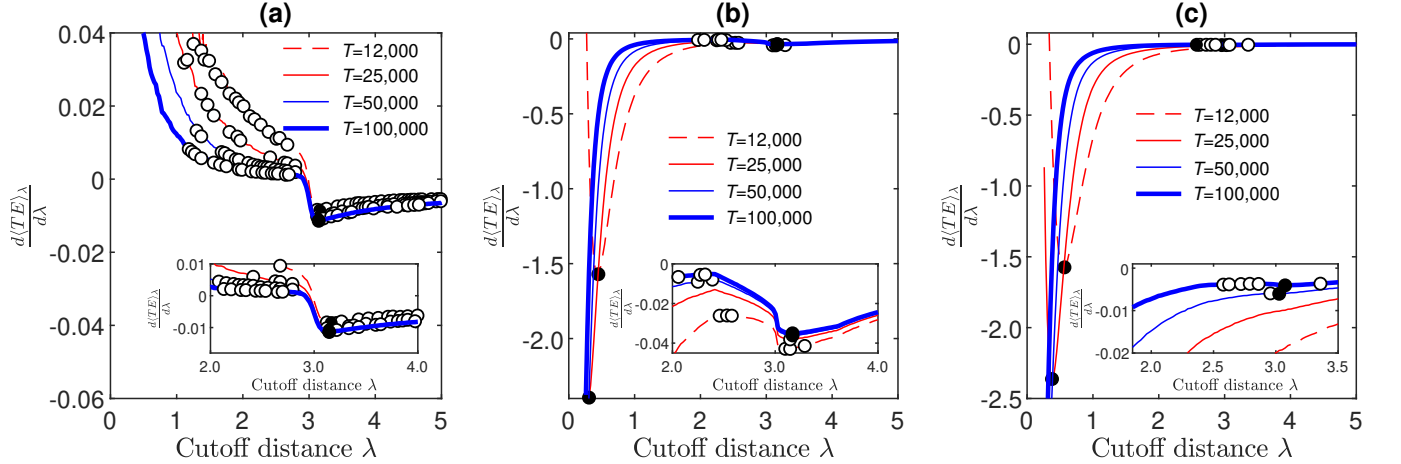


Figure 7. Derivative of average TE for different time length along with local minima and identified interaction radius based on global minimum scheme at (a)  $\eta_0 = 0.2\pi$ , (b)  $\eta_0 = 1.2\pi$  and (c)  $\eta_0 = 1.8\pi$ . The actual interaction radius  $R$  used for ensemble of trajectories is 3. Circles represent all local minima and filled-circles represent the identified interaction radius at each time length  $T$ .

contrast, when  $R$  is smaller, the  $\chi_{TE}$  distributions of leaders and followers overlap each other more with smaller variance, making the classification more difficult.

In Fig. 3(b) we set  $R = 1.0$  and varied time length and interaction strength of leader on follower  $w_{LF}$ . In this analysis followers' interaction strength is set to 1.0, i.e.,  $w_{FL} = w_{FF} = 1.0$ . Hence  $w_{LF} = 1.0$  represents no leader case that produces AUC close to 0.5 as expected. As the  $w_{LF}$  increases AUC value also increases as the leader is getting more influential on followers which makes classification easier even at short time length.

How does the predictability of interaction radius by using TE with cutoff distance depend on the number of

particles? Figure 6 represents the AUC landscape as a function of number of particles  $N$  and cutoff distance  $\lambda$ . Figure 6(a) corresponds to a fixed box size (i.e. density is changing with  $N$ ), whereas Fig. 6(b) represents the systems having same density (i.e.  $L$  is changing with  $N$ ). The actual interaction radius used to simulate the trajectories of the particles was  $R = 3$  and noise was set to  $\eta_0 = \frac{\pi}{2}$ . Although at each  $N$  the maximum AUCs are located at the underlying interaction radius  $R = 3.0$ , and the maximum AUC score is higher than the conventional no-cutoff scheme corresponding to  $R = 5\sqrt{2}$ , the maximum AUC decreases as the number of particles increases due to the increase of indirect interactions

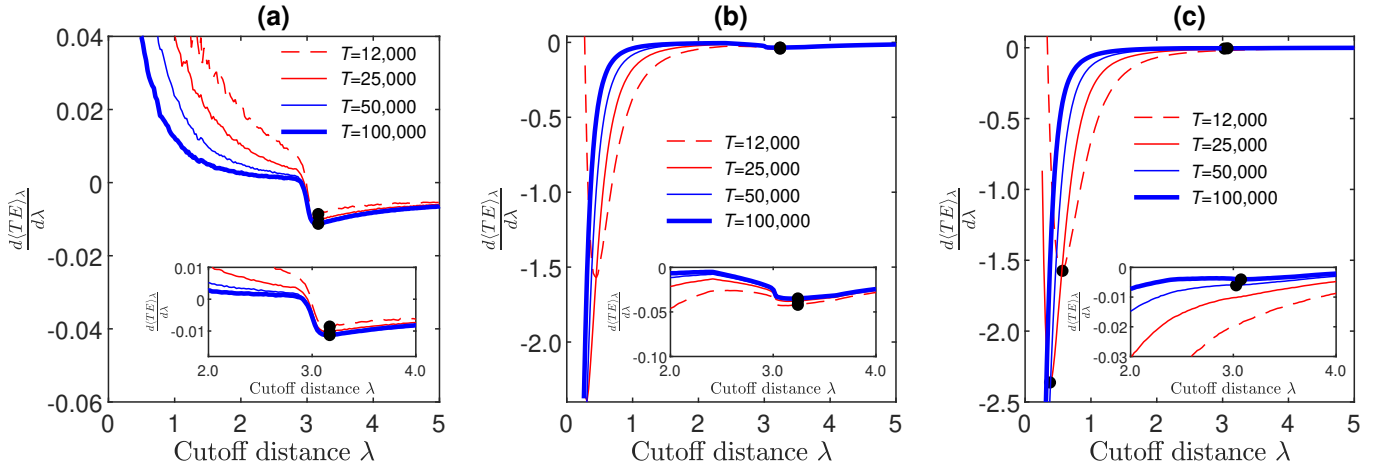


Figure 8. Derivative of average TE for different time lengths along with the identified interaction radius based on convexity score scheme at (a)  $\eta_0 = 0.2\pi$ , (b)  $\eta_0 = 1.2, \pi$  and (c)  $\eta_0 = 1.8\pi$  for  $\{n\} = \{n|1 \leq n \leq 50\}$  and  $\{M\} = \{M|2 \leq M \leq 30\}$  and  $\delta = 1 \times 10^{-6}$ .

between particles. Similar behaviors are observed at different interaction radius  $R$  and noise levels (not shown here).

How can one infer the underlying interaction radius solely from ensembles of trajectories? Recently, a simple scheme has been proposed [31] to infer the underlying interaction distance from ensembles of trajectories, based on the existence of a significant decrease in averaged transfer entropy when cutoff distance  $\lambda$  exceeds the underlying interaction radius. The interaction distance is inferred as that where the minimum of the derivatives exists along the cutoff distance  $\lambda$ :

$$\hat{R} \equiv \operatorname{argmin}_{\lambda} \frac{d\langle \text{TE} \rangle_{\lambda}}{d\lambda},$$

under the condition of  $\frac{d^2\langle \text{TE} \rangle_{\lambda}}{d\lambda^2} = 0$ . In practice, the length of trajectories may not be long enough and shorter length tends to result in a fluctuation in the course of TE along the cutoff distance  $\lambda$ , resulting in apparent minima.

Figure 7 shows the derivative of average TE as a function of cutoff distance  $\lambda$ , denoted by  $\frac{d\langle \text{TE} \rangle_{\lambda}}{d\lambda}$  for interaction radius  $R = 3$  at (a)  $\eta_0 = 0.2\pi$ , (b)  $\eta_0 = 1.2\pi$ , and (c)  $\eta_0 = 1.8\pi$  for different  $T$ . Here circles represent all local minima and the filled-circles represent the global minimum identified as the interaction radius. In Figs. 7(b) and 7(c) for relatively short  $T = 25,000$  or less,  $\frac{d\langle \text{TE} \rangle_{\lambda}}{d\lambda}$  as a function of  $\lambda$  has the global minimum at low  $\lambda$ . The locations of these global minima for short time length change with  $T$  and they vanish when  $T$  is longer, and the longer  $T = 50,000 - 100,000$  both result in a close value of the underlying interaction radius  $R = 3$ . This implies that to look for global minimum of derivative of transfer entropy may not necessarily result in an approximation of the true interaction radius especially for some short  $T$  at high noise levels.

In this paper, we present another scheme expected to be robust against fluctuations of average transfer en-

tropies along the cutoff distance by introducing a measure to quantify the degree of strong convexity at coarse-grained level, and time variance of underlying interaction radius of particles as follows.

Note in the insets of Fig. 7 that the shape of  $\frac{d\langle \text{TE} \rangle_{\lambda}}{d\lambda}$  as a function of  $\lambda$  is (strongly) convex near the actual interaction radius irrespective of time length  $T$ . This indicates that the derivative of transfer entropy as a function of cutoff distance can shed light on the underlying spatial scale of interactions among particles. However, it is not trivial to devise a scheme to automatically infer the interaction radius. Since  $\frac{d\langle \text{TE} \rangle_{\lambda}}{d\lambda}$  as a function of  $\lambda$  is convex near the interaction radius, a measure of convexity of  $\frac{d\langle \text{TE} \rangle_{\lambda}}{d\lambda}$  is versatile in determining the interaction radius. In general, due to noise,  $\frac{d\langle \text{TE} \rangle_{\lambda}}{d\lambda}$  can be fluctuated, producing apparent convex patterns locally. Thus in defining the convexity score, it is necessary to capture the non-local feature of  $\frac{d\langle \text{TE} \rangle_{\lambda}}{d\lambda}$  rather than the local feature that may be subject to noise(s). We define the convexity score  $\kappa(\lambda_i)$  of a function  $f(\lambda)$  at a point  $\lambda_i$  as  $\kappa(\lambda_i) = \frac{1}{M} \sum_{m=1}^M \sigma_i(m)$  where  $\sigma_i(m) = +1$  if  $f(\lambda_{i-m}) - f(\lambda_i) > \delta$  and  $f(\lambda_{i+m}) - f(\lambda_i) > \delta$  and  $\sigma_i(m) = -1$  if  $f(\lambda_i) - f(\lambda_{i-m}) > \delta$  and  $f(\lambda_i) - f(\lambda_{i+m}) > \delta$ , otherwise  $\sigma_i(m) = 0$ . Here  $\delta$  is a non-negative small number and  $M$  is the number of neighboring points used to determine the convexity score, and  $-1 \leq \kappa(\lambda_i) \leq 1$ . As the function of  $f(\lambda)$  we employ a simple moving averaged  $\frac{d\langle \text{TE} \rangle_{\lambda}}{d\lambda}$  with an interval  $n$ :  $f(\lambda_i) = 1/n \sum_{j=0}^{n-1} d\langle \text{TE} \rangle_{\lambda} / d\lambda |_{\lambda=\lambda_{i+j}}$ .

Thus, around a point  $\lambda_i$  where  $\frac{d\langle \text{TE} \rangle_{\lambda}}{d\lambda}$  is convex at some coarse-grained level  $\kappa(i)$  is close to unity. Hence the point  $\lambda_i$  around which  $\kappa(\lambda_i)$  is the maximum is considered to be an indicator of the interaction radius above which average transfer entropy between particles significantly decreases.

How to choose the optimal  $n$ ,  $M$ , and  $\delta$ ? We define the estimated interaction radius  $\hat{R}$  as  $\hat{R} \equiv$

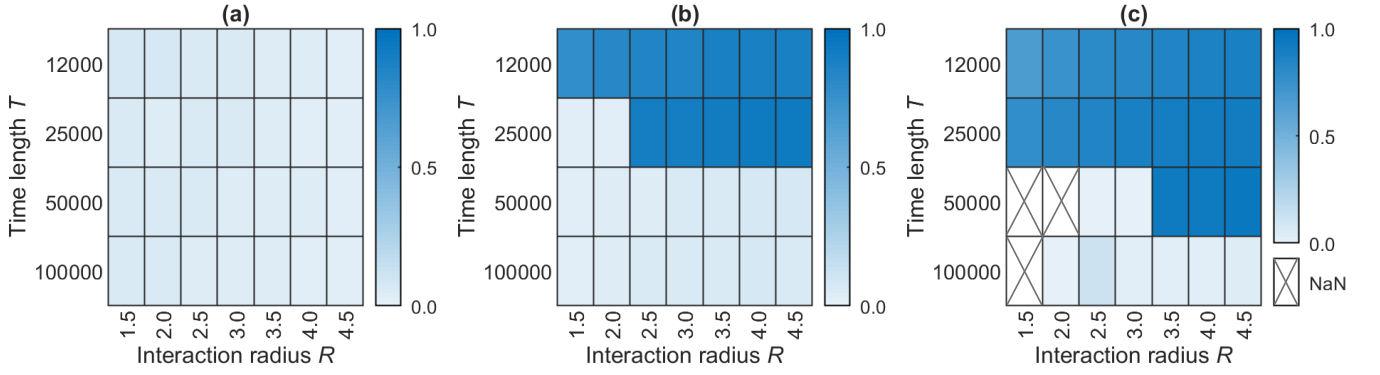


Figure 9. Relative error  $\hat{R}$  in identifying underlying interaction domain using global minimum scheme at (a)  $\eta_0 = 0.2\pi$ , (b)  $\eta_0 = 1.2\pi$ , and (c)  $\eta_0 = 1.8\pi$ . Cross-marked boxes ‘NaN’ mean that any minimum of derivatives was not detected.

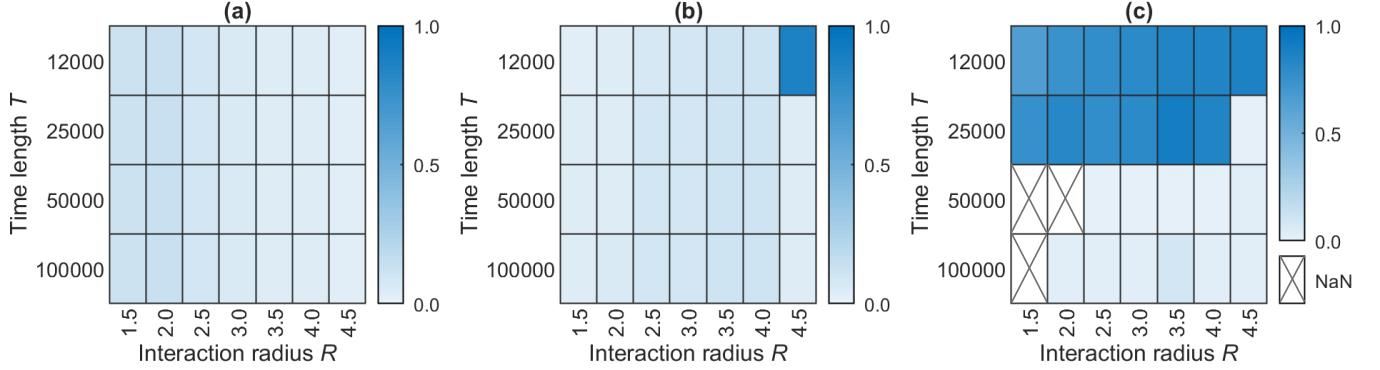


Figure 10. Relative error  $\hat{R}$  in identifying underlying interaction domain using convexity score scheme with  $\delta = 1 \times 10^{-6}$  and  $\{n\} = \{n | 1 \leq n \leq 50\}$ ,  $\{M\} = \{M | 2 \leq M \leq 30\}$  at (a)  $\eta_0 = 0.2\pi$ , (b)  $\eta_0 = 1.2\pi$ , and (c)  $\eta_0 = 1.8\pi$ . Cross-marked boxes ‘NaN’ mean that the no point was detected having non-zero convexity score  $\kappa$ .

$\operatorname{argmax}_{\lambda} \kappa(n, M; T)$ , where  $T$  represents the time length. Then the cost function is defined as

$$C(n, M) \equiv \sum_T \sum_{T'} |\hat{R}(n, M; T) - \hat{R}(n, M; T')|, \quad (4)$$

by assuming that the interaction radius is independent of time, i.e., time-invariant, and there exists (approximately) sufficient statistics for each time length in elucidating the interaction events. The parameters  $(n, M)$  is determined so that  $(n, M) = \operatorname{argmin}_{n \in \{n\}, M \in \{M\}} C(n, M)$ . Here the sets of  $n$  and  $M$  to be searched for finding optimal  $n$  and  $M$ ,  $\{n\}$  and  $\{M\}$ , are those users need to input *a priori*. Note that for some time length  $T$ ,  $\hat{R}(n, M; T)$  could not be chosen uniquely due to the degeneracy of  $\kappa(n, M; T)$  and also  $\hat{R}(n, M; T)$  could become undefined when  $\frac{d\langle TE \rangle_\lambda}{d\lambda}$  curve does not has any strongly convex part. In both the cases, we exclude such  $T$  in Eq. (4) to compute the cost function  $C(n, M)$  in defining optimal  $n$  and  $M$ . We also varied  $\delta = 0, 1 \times 10^{-8}, 1 \times 10^{-6}, 1 \times 10^{-4}$  (arb. units) and found that within this range of  $\delta$  has no significant effect on the estimation of interaction radius.

Figures 9 and 10 show the relative errors ( $\Delta R$ ) in identifying the underlying interaction domain using the

global minimum of the derivative of transfer entropy and convexity score scheme, respectively, as a function of time length and interaction radius at three different noise levels. Here relative error ( $\Delta R$ ) is defined as  $\Delta R = \frac{|R - \hat{R}|}{R}$ , where  $\hat{R}$  is the identified interaction radius using either of the two schemes.

For the global minimum (of TE derivative) scheme [Fig. 9], there exists a clear trend such that the larger the noise level the larger the relative error, and as the time length  $T$  decreases, the relative errors are more pronounced for relatively large noise levels  $\eta_0 = 1.2\pi - 1.8\pi$ . Because of the appearance of a minimum at low cutoff distance for short  $T$  that ceases to exist for longer  $T$  in Figs. 7(b) and 7(c), the global minimum scheme apparently possesses higher relative error for short  $T$  [Figs. 9 (b) and 9 (c)]. Note also that even when the time length  $T$  is sufficiently long, e.g.,  $T = 50000 - 100000$ , the global minimum scheme fails to identify the interaction radius when the noise level is highest, i.e.,  $\eta_0 = 1.8\pi$ , and interaction radius  $R$  is short, i.e.,  $R = 1.5 - 2.0$  [cross-marked boxes in Fig. 9(c)].

Figure 10 shows the relative error in identifying the interaction radius at different noise levels using convexity score scheme. Although global minimum scheme pos-



sesses high relative error at moderate noise when data length is short [Fig. 9(b)] but the convexity score scheme identifies the interaction radius satisfactorily [Fig. 10(b)]. Like the global minimum scheme, the convexity score scheme fails to identify the interaction radius when the interaction radius  $R$  is short ( $R = 1.5, 2$ ) and noise level is very high [Fig. 10(c)].

## VI. CONCLUSIONS

In this study, we examined the performance of two heuristic schemes using the derivative of transfer entropy with respect to cutoff distance  $\lambda$ ,  $\frac{d\langle TE \rangle_\lambda}{d\lambda}$ : global minimum and convexity score scheme for determining the interaction radius by using the modified VM. The striking feature -based on which we proposed the two schemes- is that  $\frac{d\langle TE \rangle_\lambda}{d\lambda}$  exhibits a kink near the actual interaction radius. A method that is capable of determining the exact location of that kink can be used in inferring interaction radius.

For short time length (at the moderate and high level of noise) for the modified VM, the derivative of average TE exhibits a minimum at low cutoff distances that produce a relatively high error for the global minimum scheme. Moreover, in real experiments it is not necessarily possible to get sufficiently long trajectories with small noises, and the global minimum scheme may yield some non-negligible error especially for short trajectories with noise. In this paper, an alternative scheme was presented, based on the property of convexity of  $\frac{d\langle TE \rangle_\lambda}{d\lambda}$  at the coarse-grained level and the assumption of time-invariance of the underlying interaction domain. For the modified VM, the scheme could capture the underlying interaction radius at the low and moderate levels of noise especially for relatively short time length, ca.  $T=12,000-25,000$  for which global minimum scheme possesses high relative error (at moderate noise level). These two heuristic schemes are compliment to each other and, as for appropriate usages, one should first visualize transfer entropy as a function of cutoff distance  $\lambda$  with its derivatives with respect to cutoff distance to confirm the existence of abrupt changes along the cutoff distance. Significant changes in the derivative of TE with respect to cutoff distance were also observed for classical trajectories of particles interacting via Lennard-Jones potential (not shown), and the existence of some significant change along cutoff distance around the typical length scale of interactions may be ubiquitous.

In systems with many variables, identifying causal relationships is a daunting task. An important aspect of systems that should be exploited, however, is that particular variable may be only influencing another particular variable at certain time instances. We have shown that filtering out those time instances where influence does not

occur greatly improves the identification of causal relationships. In the Vicsek model, for example, two agents may only interact when their distance is less than a certain threshold. To pose this as a question, we wonder at which value of interaction radius  $R$  does the motion of one agent influence the motion of another? More generally, we ponder the question: at which levels of variable  $X$  does variable  $Y$  influence variable  $Z$ ? In future work, we will demonstrate the applicability of this method by applying it to data sets stemming from different fields.

## ACKNOWLEDGMENTS

We thank Prof. A. Nakamura, Prof. M. Toda, and Prof. S. Sawai for their valuable discussions. This work was supported by a Grant-in-Aid for Scientific Research on Innovative Areas ‘‘Singularity Biology (No.8007)’’ (18H05413), MEXT, and by JSPS (No. 25287105 and 25650044 to T.K.), and JST/CREST (No. JPMJCR1662 to T.K.).

### Appendix A: Estimated interaction radius at $R = 2.0$

Figure (11) shows the derivative of average TE for different time lengths along with the identified interaction radius based on convexity score scheme at different noise levels. It has been found that at low and moderate noise levels the convexity score scheme identifies the interaction radius satisfactorily [Figs. 11(a) and 11(b)]. But at very high level of noise ( $\eta_0 \approx 1.8\pi$ ) this scheme performs satisfactorily for longer  $T$  but possesses higher relative error for shorter  $T$  [Fig. 11(c)].

### Appendix B: Convexity score

According to the definition convexity score  $\kappa$  is maximum at the point for which the  $\frac{d\langle TE \rangle_\lambda}{d\lambda}$  is strongly convex and  $\kappa$  is minimum where the curve is concave. Figure (12) shows the convexity score for very high noise level ( $\eta_0 = 1.8\pi$ ) at different interaction radii  $R$ . For  $R = 1.5$  [Fig. 12(a)] positive convexity scores have been obtained only for short  $T$  ( $T = 12,000 - 25,000$ ) which are associated with the minimum at low cutoff distance  $\lambda$ . Since  $\frac{d\langle TE \rangle_\lambda}{d\lambda}$  has no convex point for  $T = 50,000 - 100,000$  for  $R = 1.5$ , the convexity score scheme fails to identify interaction radius. For  $R = 2.0$  even though convexity score scheme fails for  $T = 50,000$  but it identifies interaction radius for  $T = 100,000$  [Fig. 12(b)]. For  $R = 2.5$  convexity score scheme can identify the interaction radius almost perfectly only for higher  $T$  ( $T = 50,000 - 100,000$ ) [Fig. 12(c)].

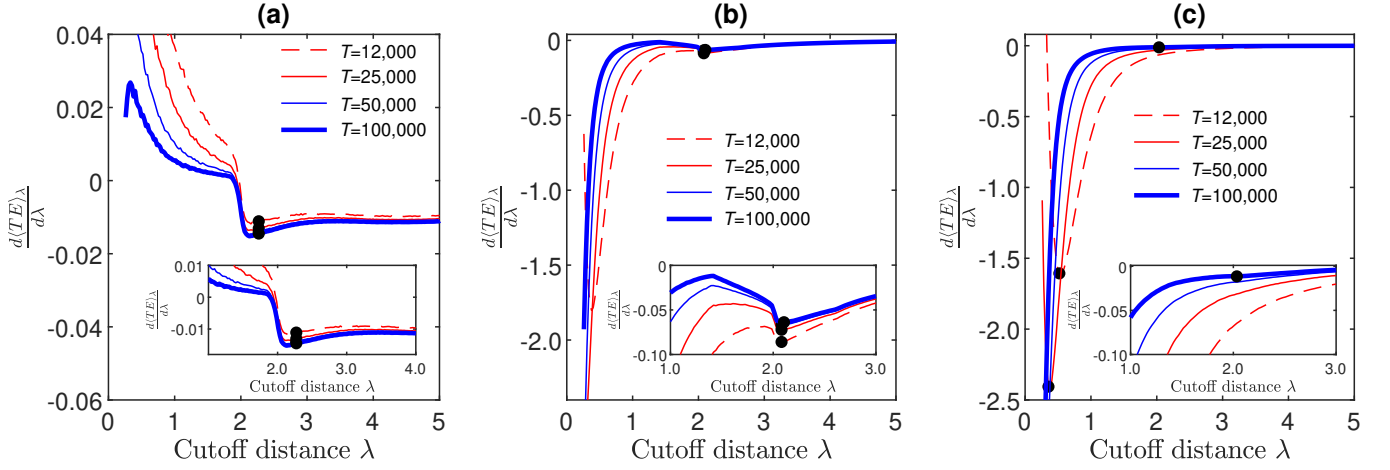


Figure 11. Derivative of average TE for different time lengths along with the identified interaction radius based on convexity score scheme at (a)  $\eta_0 = 0.2\pi$ , (b)  $\eta_0 = 1.2, \pi$  and (c)  $\eta_0 = 1.8\pi$  for  $R = 2.0$ ,  $\delta = 1 \times 10^{-6}$ , and  $\{n\} = \{n | 1 \leq n \leq 50\}$  and  $\{M\} = \{M | 2 \leq M \leq 30\}$ .

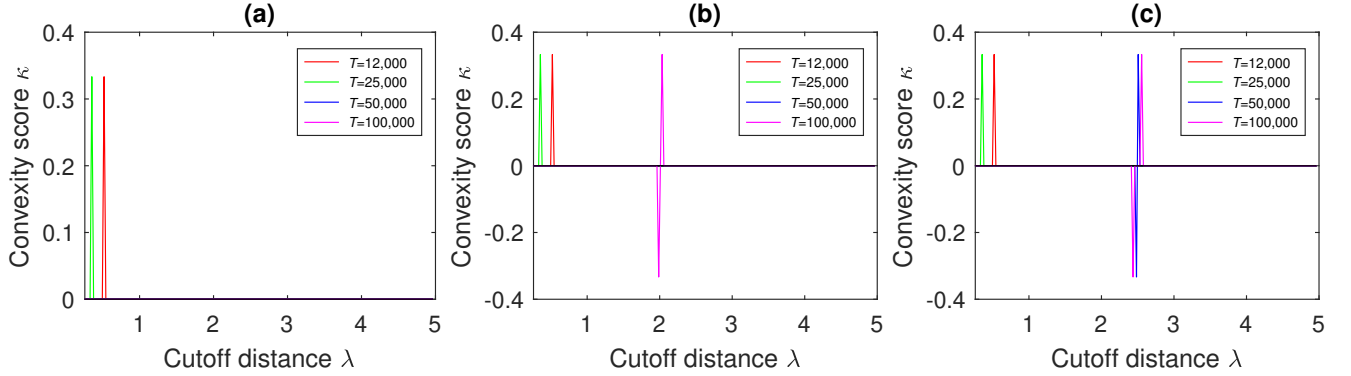


Figure 12. Convexity score  $\kappa$  at (a)  $R = 1.5$ , (b)  $R = 2.0$ , and (c)  $R = 2.5$  at  $\eta_0 = 1.8\pi$ .

- 
- [1] A. Grada, M. Otero-Vinas, F. Prieto-Castrillo, Z. Obagi, and V. Falanga, *Journal of Investigative Dermatology* **137**, e11 (2017).
- [2] E. Theveneau and C. Linker, *F1000Research* **6** (2017).
- [3] P. Friedl and D. Gilmour, *Nature reviews Molecular cell biology* **10**, 445 (2009).
- [4] A. Haeger, K. Wolf, M. M. Zegers, and P. Friedl, *Trends in cell biology* **25**, 556 (2015).
- [5] X. Trepat, M. R. Wasserman, T. E. Angelini, E. Millet, D. A. Weitz, J. P. Butler, and J. J. Fredberg, *Nature physics* **5**, 426 (2009).
- [6] W. M. Lord, J. Sun, N. T. Ouellette, and E. M. Boltt, *IEEE Transactions on Molecular, Biological and Multi-Scale Communications* **2**, 107 (2016).
- [7] C. W. Reynolds, in *Proceedings of the 14th annual conference on Computer graphics and interactive techniques* (1987) pp. 25–34.
- [8] T. Vicsek, A. Czirók, E. Ben-Jacob, I. Cohen, and O. Shochet, *Phys. Rev. Lett.* **75**, 1226 (1995).
- [9] I. D. Couzin, J. Krause, R. James, G. D. Ruxton, and N. R. Franks, *Journal of theoretical biology* **218**, 1 (2002).
- [10] W. Li, H.-T. Zhang, M. Z. Chen, and T. Zhou, *Phys. Rev. E* **77**, 021920 (2008).
- [11] A. Creppy, F. Flouraboué, O. Praud, X. Druart, S. Cazin, H. Yu, and P. Degond, *Journal of The Royal Society Interface* **13**, 20160575 (2016).
- [12] B. Szabó, G. J. Szöllösi, B. Gönci, Z. Jurányi, D. Selmeczi, and T. Vicsek, *Phys. Rev. E* **74**, 061908 (2006).
- [13] S. Butail, V. Mwaffo, and M. Porfiri, *Phys. Rev. E* **93**, 042411 (2016).
- [14] V. Mwaffo, S. Butail, and M. Porfiri, *Frontiers in Robotics AI* **4**, 35 (2017).
- [15] M. Aldana, V. Dossetti, C. Huepe, V. M. Kenkre, and H. Larralde, *Phys. Rev. Lett.* **98**, 095702 (2007).
- [16] Z. Liu and L. Guo, *Science in China Series F: Information Sciences* **51**, 848 (2008).
- [17] H. Chaté, F. Ginelli, G. Grégoire, F. Peruani, and F. Raynaud, *The European Physical Journal B* **64**, 451 (2008).
- [18] J. Krause, D. Hoare, S. Krause, C. Hemelrijk, and D. Rubenstein, *Fish and Fisheries* **1**, 82 (2000).
- [19] C. Sueur, *BMC ecology* **11**, 26 (2011).

- [20] T. D. Seeley, *The wisdom of the hive: the social physiology of honey bee colonies* (Harvard University Press, 2009).
- [21] N. Yamaguchi, T. Mizutani, K. Kawabata, and H. Haga, *Scientific reports* **5**, 1 (2015).
- [22] M. Reffay, L. Petitjean, S. Coscoy, E. Grasland-Mongrain, F. Amblard, A. Buguin, and P. Silberzan, *Biophysical journal* **100**, 2566 (2011).
- [23] T. Omelchenko, J. Vasiliev, I. Gelfand, H. Feder, and E. Bonder, *Proceedings of the National Academy of Sciences* **100**, 10788 (2003).
- [24] K. J. Cheung, E. Gabrielson, Z. Werb, and A. J. Ewald, *Cell* **155**, 1639 (2013).
- [25] K. Hlaváčková-Schindler, M. Paluš, M. Vejmelka, and J. Bhattacharya, *Physics Reports* **441**, 1 (2007).
- [26] T. M. Cover and J. A. Thomas, *Elements of information theory* (Wiley Interscience, New York, 2006).
- [27] T. Schreiber, *Phys. Rev. Lett.* **85**, 461 (2000).
- [28] J. Sun and E. M. Bollt, *Physica D: Nonlinear Phenomena* **267**, 49 (2014).
- [29] N. Orange and N. Abaid, *Eur. Phys. J.* **224**, 3279 (2015).
- [30] K. Itoda, N. Watanabe, and Y. Takefuji, *Procedia Computer Science* **71**, 85 (2015).
- [31] U. S. Basak, S. Sattari, K. Horikawa, and T. Komatsuzaki, *Phys. Rev. E* **102**, 012404 (2020).
- [32] R. G. James, N. Barnett, and J. P. Crutchfield, *Phys. Rev. Lett.* **116**, 238701 (2016).
- [33] J. A. Hanley and B. J. McNeil, *Radiology* **143**, 29 (1982).